Optimization of an ORC supersonic nozzle under epistemic uncertainties due to turbulence models

Nassim Razaaly, Giulio Gori, Gianluca Iaccarino, Pietro Congedo

Optimization of an ORC supersonic nozzle under epistemic uncertainties due to turbulence models

Nassim RAZAALY[a,*], Giulio GORI[a], Gianluca Iaccarino[c], Pietro Marco CONGEDO[a]

[a] *DeFI Team (INRIA Saclay IDF, Ecole Polytechnique), CMAP Laboratory, 1 rue d'Estienne d'Orves 91120 Palaiseau, France.*
[b] *Laboratorio di Fluidodinamica delle Macchine, Politecnico di Milano, Via Lambruschini 4, I-20156 Milano, Italy.*
[c] *Stanford University, Center for Turbulence Research, 481 Panama Mall, Stanford, CA 94305*

Abstract

Organic Rankine Cycle (ORC) turbines usually operate in thermodynamic regions characterized by high-pressure ratios and strong non-ideal gas effects in the flow expansion, complicating their aerodynamic design significantly. This study presents the shape optimization of a typical 2D ORC turbine cascade (Biere), under epistemic uncertainties due to turbulence models (RANS). A design vector of size eleven controls the blade geometry parametrized with B-splines. The EQUiPS module integrated into the SU2 CFD suite, incorporating perturbations to the eigenvalues and the eigenvectors of the modeled Reynolds stress tensor, is used to evaluate the interval estimates on the predictions of integrated Quantity of Interest (QoI), performing only five specific RANS simulations. For a given blade profile, the QoIs total loss pressure and mass flow rate, are assumed to be independent uniform random variables, defined by those estimates. A global surrogate-based method allowing to propose different designs at each optimization step is used to solve the constrained mono-objective optimization problem. To illustrate the suitability of the method, several statistics of the total pressure are considered for the minimization, under the constraint that the mean of the mass flow rate to be within a range.

Keywords: Robust Optimization, Blade Shape Optimization, SU2, Eigenspace Perturbation Methodology, Surrogate-Based Optimization, Gaussian-Processes

1. Introduction

Non-Ideal Compressible Fluid-Dynamics (NICFD) has recently been established as a new branch of fluid-mechanics [1] dealing with flows of dense vapors, supercritical fluids, and two-phase fluids, whose properties significantly depart from those of the ideal gas. In these flows, the isentropic variation of the speed of sound with density is different w.r.t. the ideal gas case.

Fluid-dynamic shape optimization (FSO) methods for design purposes have significantly improved, offering the possibility to deal with complex problems at a reduced computational cost [2]. Those methodologies play an even more critical role in the case of technologies entailing NICFD flows, where design experience and experimental information is very limited [3]. In the context of deterministic optimization, concerted research efforts have been recently devoted to develop FSO techniques for NICFD applications, such as for nozzles and turbomachinery blades, using either gradient-based [4] [5] [6] [7] or gradient-free algorithms. The latters are often coupled with surrogate models to reduce the computational cost [8] [9] [10] [11] [12]. The number of function evaluations necessary to

*Corresponding author. Tel.: +33524574177
E-mail address: nassim.razaaly@inria.fr

converge is comparatively large, and few design variables can be concurrently optimized. Nevertheless, such methods aim for a global minimum, unlike gradient-based algorithms.

The blade of interest here is a typical 2D ORC turbine cascade [13], previously studied in the context of gradient-based [4] [5] [6] or gradient-free [9] deterministic optimization.

The EQUiPS (Enabling Quantification of Uncertainty in Physics Simulations) module [14, 15] permits, in five specific RANS simulations, to perform an uncertainty quantification accounting for turbulence model inaccuracy. The robust optimization problem is recast as a *deterministic* optimization problem where the objective function to minimize is a statistics of the total pressure loss, while the mean mass flow rate is constrained to be within a given range. Three different statistics are considered here to illustrate the impact of its choice on the final result. A surrogate-based global optimization method is used to solve the problem, using the popular so-called Efficient Global Optimization algorithm [16].

The paper is organized as follows. Section 2 is devoted to the description of the design parameterization, the mesh generation/deformation and CFD simulations. In Section 3, the optimization algorithm is described. In Section 4, the optimization results are discussed, and the evidence about the interest of the proposed framework is provided. Conclusions and some perspectives are then provided in Section 5.

2. Blade Parametrization and CFD settings

2.1. Design vector: Blade Parametrization

In order to reconstruct the 2D blade profile employing a minimum number of variables, an unique B-spline curve is used to parametrize both pressure and suction sides of the cascade. An exhaustive description of B-splines curves/surfaces can be found in [17] [18]. The trailing edge is considered fixed separately, approximated by a circular arc. A B-spline curve $p(t)$ of degree n can be written as

$$p(t) = \sum_{i=0}^{n} N_{i,k}(t)\mathbf{a}_i, \tag{1}$$

where $\mathbf{a}_i$ denotes the i-th control point (CP) with $i \in [\![0, n]\!]$. $N_{i,k}(t)$ is the corresponding $k-1$ degree polynomial B-Spline basis function, defined recursively by:

$$\begin{aligned} N_{i,1}(t) &= \mathbf{1}_{[t_i, t_{i+1}[}(t) \\ N_{i,k}(t) &= \frac{t - t_i}{t_{i+k-1} - t_i} N_{i,k-1}(t) + \frac{t_{i+k} - t}{t_{i+k} - t_{i+1}} N_{i+1,k-1}(t), \end{aligned} \tag{2}$$

where $\{t_j\}_{j \in [\![0, n+k]\!]}$ denotes the increasing so-called knot sequence, and $t \in [t_{k-1}, t_{n+1}]$ is a scalar parametrising the B-Spline curve.

11 CP are allowed to move in the normal direction to the blade (Figure 1). In order to control the trailing edge thickness, the four CP's displacements located at the latter are linked to each other. Therefore, the blade geometry is controled by a design vector $\mathbf{x} \in \mathbb{R}^d$, $d = 11$.

2.2. Mesh

Mesh Generation. The numerical grids are generated using an in-house tool based on an advancing-front/Delaunay algorithm. To create hybrid grids suitable for viscous simulations, quadrilateral elements are first added over the solid walls, to build a boundary layer mesh. Since the flow features the typical fish-tail shock patter at the blade trailing edge, grids were slightly refined in regions where shocks were expected to develop.

Grid Deformation using RBF. In this study, we rely on the use of a grid deformation strategy in order to accurately deform the grid for an assigned boundary displacement. The present approach follows the work of [19], successfully

(a) Blade Parametrization

(b) Zoom at Trailing Edge.

Figure 1: Baseline profile approximated by B-splines: 30 CP, 11 Free CP (red), 19 Fixed CP (black).

applied in [20], to achieve a highly flexible and robust deformation tool for unstructured meshes, based on the interpolation of boundary nodes displacements to the whole mesh with Radial Basis Function (RBF's). A linear system of equations only involving boundary nodes has to be solved, and no grid connectivity information is needed. The RBF retained in this work is the so-called *Volume* function, with global support, defined by $\Phi(r) = r$.

2.3. CFD

2.3.1. RANS Solver

The Non-Ideal Computational Fluid-Dynamics (NI-CFD) solver included in the SU2 [21, 22] suite is employed in this work, its reliability being assessed in [23–25]. In the following, a brief overview of its main features are highlighted. The three-dimensional Navier-Stokes equations for compressible flows read

$$\frac{\partial \mathbf{u}}{\partial t} + \nabla \cdot \mathbf{f}(\mathbf{u}) = \nabla \cdot \mathbf{d}(\mathbf{u}) \tag{3}$$

The vector of the conserved variables $\mathbf{u} = (\rho, \mathbf{m}, E^t)^T$ includes the mass density $\rho \in \mathbb{R}^+$, the three component vector related to momentum density $\mathbf{m} \in \mathbb{R}^3$, and the total energy density per unit of volume $E^t \in \mathbb{R}$, $E^t = \rho\left(e + \frac{1}{2}\|\mathbf{v}\|^2\right)$ (where e is the internal energy per unit mass while $\mathbf{v} = \mathbf{m}/\rho$ is the velocity vector).

The functions $\mathbf{f}(\mathbf{u}) = [\mathbf{m}, (\mathbf{m}\otimes\mathbf{m})/\rho + P\mathbf{I}, \mathbf{m}(E^t + P)/\rho]^T$ and $\mathbf{d}(\mathbf{u}) = [\mathbf{0}, \mathbf{\Pi}, \mathbf{v}^T \cdot \mathbf{\Pi} - \mathbf{q})]^T \in \mathbb{R}^5 \times \mathbb{R}^3$ are, respectively, the hypervector of the advection and pressure fluxes and the hypervector of the viscous and thermal fluxes. In these latter functions, $P = P(\mathbf{u})$ is the pressure, $\mathbf{I}$ is the identity matrix, $\mathbf{\Pi} = \mathbf{\Pi}(\mathbf{v})$ is the viscous stress tensor and $\mathbf{q}$ is the thermal flux.

The system of equations is supplemented by constitutive relations that bound the state of the fluid to the thermodynamic and to the transport quantities. The behavior of the fluid of interest (MDM Table 1) is described using the Peng-Robinson (PR) Equation of State (EOS). Non-Reflecting Boundary Conditions (NRBC) [26], designed to avoid spurious pressure oscillations due to the reflection of acoustic waves at the domain boundaries, are exploited to perform computations on a truncated domain, with multigrid techniques, lowering the computational burden. A second order approximate Riemann solver (ARS) of Roe upwind type [27–29] is used along with the slope limiter proposed by van Albada. The Menters Shear Stress Transport (SST) [30] model is used to retrieve the effects of turbulence in RANS simulations. Nominal operating conditions for total inlet pressure and temperature, and outlet static pressure are provided in Table 2.

Critical pressure	1.41 MPa
Critical temperature	564.1 K
γ	1.0165
Acentric factor ω	0.529
Gas constant	35.15 J/kg/K

Table 1: Peng-Robinson Parameters for the MDM Siloxane.

	P^t_{in}	T^t_{in}	P^s_{out}
Nominal	8 bars	545.15 K	1.072 bars

Table 2: Nominal Operating Conditions.

The performance parameters considered are the total pressure loss $Y = \dfrac{P^t_{in} - P^t_{out}}{P^t_{in} - P^s_{out}}$, and the mass flow rate $\dot{m}$.

2.3.2. QoI Interval Estimates using the EQUiPS module

Due to the simplifications invoked in model formulation, RANS models can only represent certain features of turbulence with limited fidelity. In this paper, the EQUiPS module [14, 15] is used to estimate interval bounds of engineering QoI based on only five perturbed RANS simulations. The so-called Eigenspace Perturbation Methodology (EPM) performs sequential perturbations on the eigenvalues and eigenvectors of the modeled Reynods stress tensor to estimate turbulence model discrepancy. For a given profile parameterized by $\mathbf{x}$, five independent RANS simulations are performed. The QoIs are post-processed: $\{\dot{m}_i(\mathbf{x}), Y_i(\mathbf{x})\}_{i\in[\![1,5]\!]}$. Interval bounds are simply evaluated as:

$$\begin{aligned} \dot{m}_{min} &= \operatorname*{Min}_i \ \dot{m}_i(\mathbf{x}) & \dot{m}_{max} &= \operatorname*{Max}_i \ \dot{m}_i(\mathbf{x}) \\ Y_{min} &= \operatorname*{Min}_i \ Y_i(\mathbf{x}) & Y_{max} &= \operatorname*{Max}_i \ Y_i(\mathbf{x}) \end{aligned} \tag{4}$$

Note that $i_0 = \arg\min_i \ Y_i(\mathbf{x})$ does not imply that $i_0 = \arg\min_i \ \dot{m}_i(\mathbf{x})$.

2.3.3. Settings

A mesh of size 37k Elements is selected for the optimization procedure. A dedicated grid analysis performed at nominal conditions (without EPM) shows that QoI's relative errors is around 7%, w.r.t. the grid independent solution. A representation of the blade shape, alongside the computational mesh, is given in Figure 2. An adaptative CFL is selected to be between 10 and 50. Simulations are assumed to be converged when residuals on the density are decreased by six orders of magnitude, or after 7000 iterations. Ill-converged simulations are re-run automatically with a minimal CFL of 1. Each RANS simulations is performed with one core, on the Stanford cluster *Certainty* equipped with Intel(R) Xeon(R) CPU X5650 at 2.67GHz.

3. Optimization

3.1. Optimization Formulation

In order to perform the optimization under the epistemic uncertainty due to turbulence models, the problem is reformulated in a stochastic framework. For each design vector $\mathbf{x}$ describing the blade geometry, the QoI $Y(\mathbf{x})$ and $\dot{m}(\mathbf{x})$ are assumed to be independent uniform random variables defined by their respective interval bounds $Y_{min}(\mathbf{x})$, $Y_{max}(\mathbf{x})$, $\dot{m}(x)_{min}(\mathbf{x})$ and $\dot{m}(x)_{max}(\mathbf{x})$, evaluated with the EQUiPS module. Within these assumptions, all statistics are explicit functions of the interval bounds.

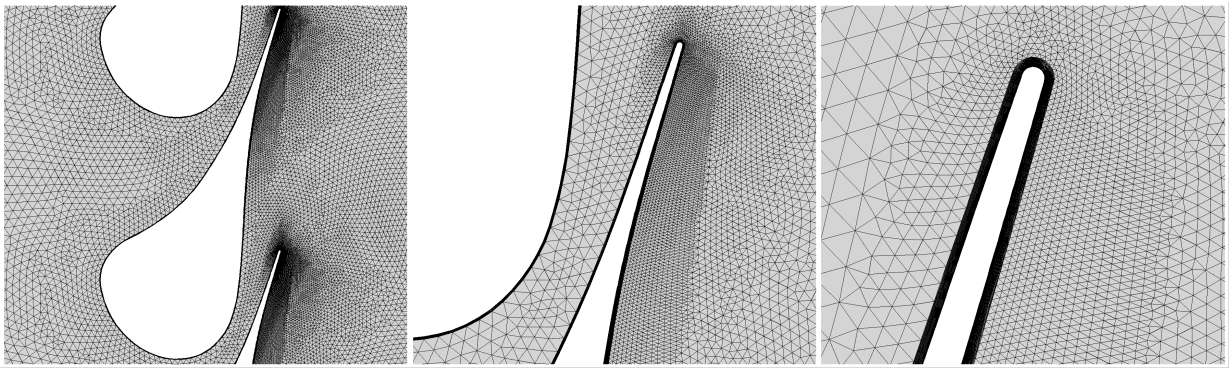

(a) (b) (c)

Figure 2: 37k Elements mesh.

The following statistics of the total pressure $Y(\mathbf{x})$ are successively optimized, subject to the mean mass flow rate constrained to be within a range centered around the baseline value:

- The mean $\mu_Y(\mathbf{x}) = \dfrac{Y_{min}(\mathbf{x}) + Y_{max}(\mathbf{x})}{2}$, accounting only for average performances only.
- A weighted sum of the mean and the range $\mu_Y(\mathbf{x}) + \Delta_Y(\mathbf{x})$, with $\Delta_Y(\mathbf{x}) = Y_{max}(\mathbf{x}) - Y_{min}(\mathbf{x})$.
- The 95%-quantile (a high quantile) $q_Y^{95}(\mathbf{x}) = Y_{min}(\mathbf{x}) + 0.95\Delta_Y(\mathbf{x})$

The two latters aim at both minimize the average and reduce the variability inherent to the turbulence model. Of course, other statistics rewritten as a linear combinaison of the interval bounds could have been selected. The corresponding constrained mono-objective formulation read:

$$\begin{aligned} &\text{Minimize} \quad f_Y(\mathbf{x}) \\ &\quad \text{s.t.} \quad \mu_{\dot{m}}(\mathbf{x}) \in [\dot{m}_b \pm \Delta\dot{m}_b] \\ &\qquad \mathbf{x} \in [\mathbf{x}_{min}, \mathbf{x}_{max}] \end{aligned} \tag{5}$$

where f_Y denotes μ_Y, $\mu_Y + \Delta_Y$ or q_Y^{95}, $\mu_{\dot{m}}(\mathbf{x}) = \dfrac{\dot{m}_{min}(\mathbf{x}) + \dot{m}_{max}(\mathbf{x})}{2}$. $\dot{m}_b$ and $\Delta\dot{m}_b$ denote respectively a prescribed mass flow rate value (here the baseline one) and a range.

3.2. Surrogate-based Optimization

To solve the constrained optimization problem Equation 6, a surrogated-based method combining the popular so-called Efficient Global Optimization (EGO) [16] and Gaussian Processes (GP) (see [31] for details) is used.
An initial Design of Experiment (DoE) of size n_{LHS} is built based on Latin Hypercube Sampling (LHS): $\{\mathbf{x}_i\}_{i\in[\![1,n_{LHS}]\!]}$. For each design parametrized by the vector $\mathbf{x}_i \in \mathbb{R}^d$, five RANS simulations are performed (EPM), so interval bounds for the total pressure loss $Y(\mathbf{x}_i)$ and the mass flow rate $\dot{m}(\mathbf{x}_i)$ are post-processed. The objective/constraint functions $f_Y(\mathbf{x}_i)$ and $\mu_{\dot{m}}(\mathbf{x}_i)$ are therefore easily obtained.
Two GP surrogate for the objective/constraint function are built from the DoE: $\tilde{f}_Y(\mathbf{x})$ and $\tilde{\mu}_{\dot{m}}(\mathbf{x})$. An anisotropic Matern $\dfrac{5}{2}$ kernel is selected. The problem is then re-written as:

$$\begin{aligned} &\text{Minimize} \quad \tilde{f}_Y(\mathbf{x}) \\ &\quad \text{s.t.} \quad \tilde{\mu}_{\dot{m}}(\mathbf{x}) \in [\dot{m}_b \pm \Delta\dot{m}_b] \\ &\qquad \mathbf{x} \in [\mathbf{x}_{min}, \mathbf{x}_{max}] \end{aligned} \tag{6}$$

A new design maximizing the so-called *Expected Improvement* (EI), accounting for the gaussian nature of the surrogate, is iteratively added to the DoE, updating *a posteriori* the two GP-surrogates.
Note that in this study, the same initial DoE is used for solving the three optimizations problems. The list of parameters used in that study are summarized in Table 3.2.

n_{LHS}	$\dot{m}_b$	$\Delta\dot{m}_b$
100	14.9 kg/s/m	$0.05\dot{m}_b$

Table 3: Tuning Parameters

4. Results

Three optimization problems with the same constraint function $\dot{m}(\mathbf{x})$ are solved, with objective functions $f_Y(\mathbf{x})$ representing different statistics of the assumed random variable $Y(\mathbf{x})$: its mean $\mu_Y(\mathbf{x})$, its quantile $q_Y^{95}(\mathbf{x})$ and a weighted sum of the mean and the range $\mu_Y(\mathbf{x})+\Delta_Y(\mathbf{x})$. The respective optimization results are illustrated respectively in Figures 3, 4 and 5. The Mach contours are represented for the optimized blade (standard RANS simulation), and a convergence history of the objective function is provided: the best objective function evaluated by CFD (EPM) is plot in bold black line as a function of the number of profiles considered. Corresponding interval bounds of the total pressure loss are also shown to illustrate the optimization strategy. A vertical blue line indicates the initial DoE size.
The same initial DoE is used for solving the three optimization problems. The total pressure loss interval bounds for the baseline profile are $[18.1, 19.3]\%$.

Minimization of $\mu_Y(\mathbf{x})$. The optimized profile in that case gives a total pressure loss of $Y \in [8.46, 9.80]\%$, which is significantly lower than the one of the baseline profile. After the initial DoE evaluation and the GP building of both the objective and constraint functions, the mean $\mu_Y(\mathbf{x})$ is decreased quite fast, the optimal profile obtained after 150 profiles evaluations (750 RANS simulations).

Minimization of $\mu_Y(\mathbf{x}) + \Delta_Y(\mathbf{x})$. The optimized profile in that case gives a total pressure loss of $Y \in [9.07, 10.24]\%$, which mean value is higher than in the case of minimizing the mean, but with a lower range, 1.11%, against 1.34%. The objective function in black is, as expected, above the upper bound of Y. Interestingly, the convergence history shows a decrease followed by an increase of the lower bound, twice, while the objective function decreases. Indeed, those increases of the lower bound coincide with an increase of the range, explaining that behaviour, while a following profile exhibits a lower range but a higher lower bound. The converge is much slower, with an optimal profile obtained after more than 200 profiles. It seems that including the range in the objective function, as such deteriorates the quality of the surrogate model, explaining the poor convergence.

Minimization of $q_Y^{95}(\mathbf{x})$. The optimized profile in that case gives a total pressure loss of $Y \in [7.78, 9.33]\%$, with bounds lower than the ones obtained for the optimizations performed above. The objective function in black is as expected very close to the upper bound of Y. The convergence rate is much faster, the optimal profile obtained after only 125 profiles, 25 iterations after the initial DoE.

5. Conclusion

Due to the limited design experience and to the limited experimental information on NICFD flows, the design of ORC turbine cascade can greatly benefit from automated dynamic shape optimization techniques, taking into account of uncertainties in the context of robust optimization. A Robust Optimization method accounting for the uncertainties due to turbulence models were fully documented and applied to the design of a supersonic ORC cascade operating in the NICFD regime. No uncertainties on operating conditions or geometric tolerances are taken into consideration. The EQUiPS module, based on the Eigenspace Perturbation Methodology, was used to perform an uncertainty quantification accounting for turbulence models inaccuracy in five RANS simulations, for a given blade profile. The

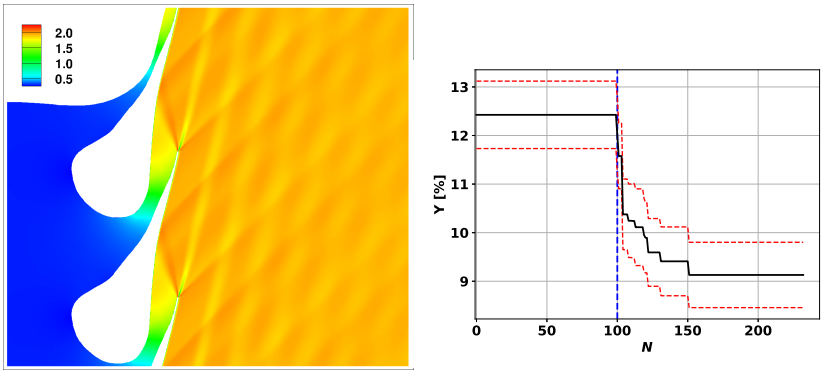

(a) Mach Contours (b) Convergence History

Figure 3: Minimization of the mean μ_Y results. $Y \in [8.46, 9.80]\%$.

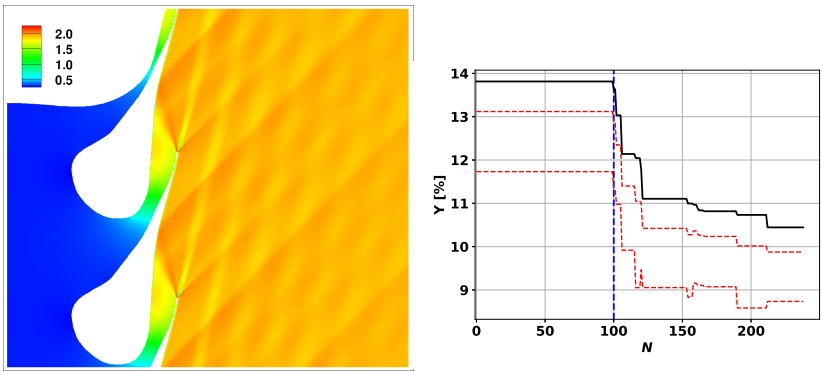

(a) Mach Contours (b) Convergence History

Figure 4: Minimization of the weighted sum $\mu_Y + \Delta_Y$ results. $Y \in [9.07, 10.24]\%$.

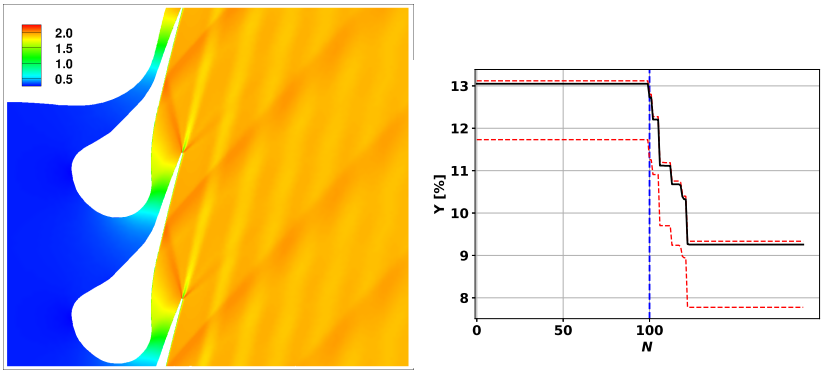

(a) Mach Contours. (b) Convergence History

Figure 5: Minimization of the 95%-quantile q_Y^{95} results. $Y \in [7.78, 9.33]\%$.

initial robust optimization problem was reformulated as a *deterministic* optimization where the objective function is a statistics of the total pressure loss, while the mean mass flow rate is constrained to be within a given range.
In this framework, both the total pressure loss and the mass flow rate are modeled as independent uniform random

variables defined by their respective interval bounds, post-processed from the EQUiPS simulations.
Three different statistics of the total pressure loss (mean, mean plus range, 95%-quantile) are considered yielding to three different optimization methods for illustrating the importance of the choice of the robust optimization formulation. All of them are solved using a popular surrogate-based technique combining Gaussian Processes and the maximization of the so-called *Expected Improvement*. Note that this global optimization method is sharply limited by the ability of the surrogate model to fit the original objective function, and is suitable due to the low dimension of the design space (11). The capability of the proposed method was demonstrated by redesigning a typical 2D ORC turbine cascade. The methodology permitted to improve the cascade performances substantially, for all statistics considered. Note that for the proposed problem, a classic adjoint-based method involving a Newton-like optimization method cannot be applied straightforwardly, since the objective/constraint functions are not differentiable.

Future work will be devoted to the extension of the proposed approach taking benefits from the adjoint method available in the SU2 package to further reduce the computational burden.

References

[1] NICFD, . 1st International Seminar on Non-Ideal Compressible-Fluid Dynamics for Propulsion and Power. http://nicfd2016.polimi.it; 2016.

[2] Pironneau, O.. On optimum design in fluid mechanics. Journal of Fluid Mechanics 1974;64(1):97110. doi:10.1017/S0022112074002023.

[3] Harinck, J., Pasquale, D., Pecnik, R., van Buijtenen, J., Colonna, P.. Performance improvement of a radial organic rankine cycle turbine by means of automated computational fluid dynamic design. Proceedings of the Institution of Mechanical Engineers, Part A: Journal of Power and Energy 2013;227(6):637–645.

[4] Pini, M., Persico, G., Pasquale, D., Rebay, S.. Adjoint method for shape optimization in real-gas flow applications. ASME Journal of Engineering for Gas Turbines and Power 2015;137(3).

[5] Pini, M., Persico, G., Dossena, V.. Robust adjoint-based shape optimization of supersonic turbomachinery cascades. In: ASME Turbo Expo 2014: Turbine Technical Conference and Exposition. American Society of Mechanical Engineers; 2014, p. V02BT39A043–V02BT39A043.

[6] Vitale, S., Albring, T.A., Pini, M., Gauger, N.R., Colonna, P., et al. Fully turbulent discrete adjoint solver for non-ideal compressible flow applications. Journal of the Global Power and Propulsion Society 2017;1:Z1FVOI.

[7] Rubino, A., Pini, M., Colonna, P., Albring, T., Nimmagadda, S., Economon, T., et al. Adjoint-based fluid dynamic design optimization in quasi-periodic unsteady flow problems using a harmonic balance method. Journal of Computational Physics 2018;.

[8] Quagliarella, D.. Genetic algorithms and evolution strategy in engineering and computer science: recent advances and industrial applications. John Wiley & Son Ltd; 1998.

[9] Rodriguez-Fernandez, P., Persico, G.. Automatic design of ORC turbine profiles using evolutionary algorithms. 3rd International Seminar on ORC Power Systems 2015;(133).

[10] Pierret, S., Coelho, R.F., Kato, H.. Multidisciplinary and multiple operating points shape optimization of three-dimensional compressor blades. Structural and multidisciplinary optimization 2007;33(1):61–70.

[11] Samad, A., Kim, K.. Shape optimization of an axial compressor blade by multi-objective genetic algorithm. Proceedings of the Institution of Mechanical Engineers, Part A: Journal of Power and Energy 2008;222(6):599–611.

[12] Samad, A., Kim, K.Y., Goel, T., Haftka, R.T., Shyy, W.. Multiple surrogate modeling for axial compressor blade shape optimization. Journal of Propulsion and Power 2008;24(2):301–310.

[13] Colonna, P., Harinck, J., Rebay, S., Guardone, A.. Real-gas effects in organic rankine cycle turbine nozzles. Journal of Propulsion and Power 2008;24(2):282–294.

[14] Mishra, A.A., Iaccarino, G.. Uncertainty estimation for reynolds-averaged navier–stokes predictions of high-speed aircraft nozzle jets. AIAA Journal 2017;:3999–4004.

[15] Iaccarino, G., Mishra, A.A., Ghili, S.. Eigenspace perturbations for uncertainty estimation of single-point turbulence closures. Physical Review Fluids 2017;2(2):024605.

[16] E. Brochu, V.M.C., de Freitas, N.. A tutorial on bayesian optimization of expensive cost functions, with application to active user modeling and hierarchical reinforcement learning. arXiv:10122599 2010;.

[17] Hoschek, J., Lasser, D., Schumaker, L.L.. Fundamentals of computer aided geometric design. AK Peters, Ltd.; 1993.

[18] Farin, G.. Curves and Surfaces for CAGD: A Practical Guide. 5 ed.; San Francisco, CA, USA: Morgan Kaufmann Publishers Inc.; 2002.

[19] De Boer, A., Van der Schoot, M., Bijl, H.. Mesh deformation based on radial basis function interpolation. Computers & structures 2007;85(11-14):784–795.

[20] Pini, M.. Turbomachinery design optimization using adjoint method and accurate equations of state. Ph.D. thesis; Politecnico di Milano; 2013.

[21] Palacios, F., Colonno, M.F., Aranake, A.C., Campos, A., Copeland, S.R., Economon, T.D., et al. Stanford University Unstructured (SU2): An open-source integrated computational environment for multi-physics simulation and design. In: 51st AIAA Aerospace Sciences Meeting and Exhibit. 2013,.

[22] Economon, T.D., Mudigere, D., Bansal, G., Heinecke, A., Palacios, F., Park, J., et al. Performance optimizations for scalable implicit {RANS} calculations with {SU2}. Computers & Fluids 2016;129:146 – 158. URL: http://www.sciencedirect.com/science/article/pii/S0045793016300214. doi:http://dx.doi.org/10.1016/j.compfluid.2016.02.003.

[23] Gori, G., Guardone, A., Vitale, S., Head, A., Pini, M., Colonna, P.. Automatic design of ORC turbine profiles using evolutionary algorithms. 3rd International Seminar on ORC Power Systems 2015;(133).

[24] Pini, M., Vitale, S.,, , Colonna, P., Gori, G., Guardone, A., et al. Su2: the open-source software for non-ideal compressible flows. In: NICFD 2016: 1st International Seminar on Non-Ideal Compressible-Fluid Dynamics for Propusion & Power. Varenna, Italy; 2016,.
[25] Gori, G., Zocca, M., Cammi, G., Spinelli, A., Guardone, A.. Experimental assessment of the open-source su2 cfd suite for orc applications. Energy Procedia 2017;129(Supplement C):256 – 263. doi:https://doi.org/10.1016/j.egypro.2017.09.151.
[26] Giles, M.B.. Nonreflecting boundary conditions for euler equation calculations. AIAA journal 1990;28(12):2050–2058.
[27] Roe, P.L.. Approximate riemann solvers, parameter vectors, and difference schemes. J Comput Phys 1981;43(2):357–372. URL: http://linkinghub.elsevier.com/retrieve/pii/0021999181901285.
[28] Vinokur, M., Montagné, J.L.. Generalized flux-vector splitting and roe average for an equilibrium real gas. J Comput Phys 1990;89:276.
[29] Guardone, A., Vigevano, L.. Roe linearization for the van der Waals gas. J Comput Phys 2002;175:50–78.
[30] Menter, F.. Zonal two equation kw turbulence models for aerodynamic flows. In: 23rd fluid dynamics, plasmadynamics, and lasers conference. 1993, p. 2906.
[31] Rasmussen, C.E.. Gaussian processes in machine learning. In: Advanced lectures on machine learning. Springer; 2004, p. 63–71.